

Thermodynamic stability of small-world oscillator networks: A case study of proteins

Jie Ren* and Baowen Li†

*NUS Graduate School for Integrative Sciences and Engineering, Singapore 117597, Republic of Singapore and
Department of Physics and Centre for Computational Science and Engineering,
National University of Singapore, Singapore 117542*

(Dated: February 3, 2022)

We study vibrational thermodynamic stability of small-world oscillator networks, by relating the average mean-square displacement S of oscillators to the eigenvalue spectrum of the Laplacian matrix of networks. We show that the cross-links suppress S effectively and there exist two phases on the small-world networks: 1) an unstable phase: when $p \ll 1/N$, $S \sim N$; 2) a stable phase: when $p \gg 1/N$, $S \sim p^{-1}$, *i.e.*, $S/N \sim E_{cr}^{-1}$. Here, p is the parameter of small-world, N is the number of oscillators, and $E_{cr} = pN$ is the number of cross-links. The results are exemplified by various real protein structures that follow the same scaling behavior $S/N \sim E_{cr}^{-1}$ of the stable phase. We also show that it is the “small-world” property that plays the key role in the thermodynamic stability and is responsible for the universal scaling $S/N \sim E_{cr}^{-1}$, regardless of the model details.

PACS numbers: 87.14.E-, 05.40.-a, 89.75.-k

Vibrational dynamics has been widely used to study thermodynamic properties of various structures in solid state physics and/or other disciplines [1]. Since the structure is considered as a primary factor responsible for physical properties, to keep the underlying structure thermally stable is of primary important for systems to function properly. For example, proteins, comprising an extremely heterogeneous class of biological macromolecules, must be stable enough against thermal fluctuations and/or external perturbations so as to maintain their native structures and to function correctly [2, 3]. Therefore, a natural and important question is often asked: what is the structure effect on thermodynamic stability? In this paper, we study the stability of small-world structures [4], which is then exemplified by proteins.

The dynamics of N coupled oscillators on the network in contact with the external heat reservoir can be expressed as:

$$M\ddot{q} = -\sigma Lq - \Gamma\dot{q} + \xi \quad (1)$$

where $q = [q_1, q_2, \dots, q_N]^T$, denotes the oscillator's displacements from the equilibrium positions. $M_{ij} = m_i \delta_{ij}$ is the mass matrix, where m_i denotes the mass of the i th oscillator. σ is the spring constant. $L_{ij} = \delta_{ij} \sum_m A_{im} - A_{ij}$ is the Laplacian matrix and A_{ij} is the adjacency matrix of the network, where $A_{ij} = 1$ if i and j are connected and $A_{ij} = 0$ otherwise. $\Gamma_{ij} = \gamma_i \delta_{ij}$ is the dissipation matrix where γ_i is the dissipation coefficient of the i th oscillator influenced by the heat reservoir. Vector $\xi = [\xi_1, \xi_2, \dots, \xi_N]^T$ denotes the thermal fluctuation with zero mean and variance $\langle \xi_i(t) \xi_j(t') \rangle = 2k_B T \Gamma_{ij} \delta(t - t')$, which is the usual fluctuation-dissipation relation.

The harmonic potential we adopt looks very simple but can capture the main features of the system. For example, Tirion [5] demonstrates that a single-parameter harmonic potential can reproduce vibrational properties of the real macromolecular system very well. Thereafter, the Gaussian network model (GNM) [6] has been widely used in protein research and yields results in good agreement with experiments. In the GNM model, the interactions are considered as homogeneous harmonic springs, which is in analogy with the elasticity theory of random polymer networks [7, 8].

The correlation matrix of oscillator displacements at the steady state for Eq. (1) can be easily obtained (see Appendix A):

$$C_{lk} = \langle q_l q_k \rangle = \frac{k_B T}{\pi} \int_{-\infty}^{+\infty} d\omega [G^{-1}(i\omega) \Gamma G^{-1}(-i\omega)]_{lk}, \quad (2)$$

where matrix $G(\pm i\omega) = (\pm i\omega)^2 M + (\pm i\omega) \Gamma + \sigma L$. Since $G(i\omega) - G(-i\omega) = 2i\omega \Gamma$ and $G(0) = \sigma L$, one can eliminate Γ in the above integral and obtain:

$$C = -\frac{k_B T}{\pi i} \int_{-\infty}^{+\infty} \frac{d\omega}{\omega} G^{-1}(i\omega) = \frac{k_B T}{\sigma} L^\dagger, \quad (3)$$

where L^\dagger denotes the pseudo-inverse of L . It excludes zero mode which corresponds to the translational invariance of the system, and is the inverse of L in the subspace orthogonal to the zero mode:

$$L_{ij}^\dagger = \sum_{\alpha=1}^{N-1} \frac{1}{\lambda_\alpha} \psi_{\alpha i} \psi_{\alpha j}, \quad (4)$$

where λ_α are the non-zero eigenvalues, and $\psi_{\alpha j}$ denote the corresponding normalized eigenvectors of L . Therefore, we can obtain the average mean-square displacement straightforwardly:

$$S = \frac{1}{N} \sum_i \langle q_i^2 \rangle = \frac{1}{N} \text{tr} C = \frac{k_B T}{N\sigma} \sum_{\alpha=1}^{N-1} \frac{1}{\lambda_\alpha}. \quad (5)$$

*Electronic address: renjie@nus.edu.sg

†Electronic address: phylibw@nus.edu.sg

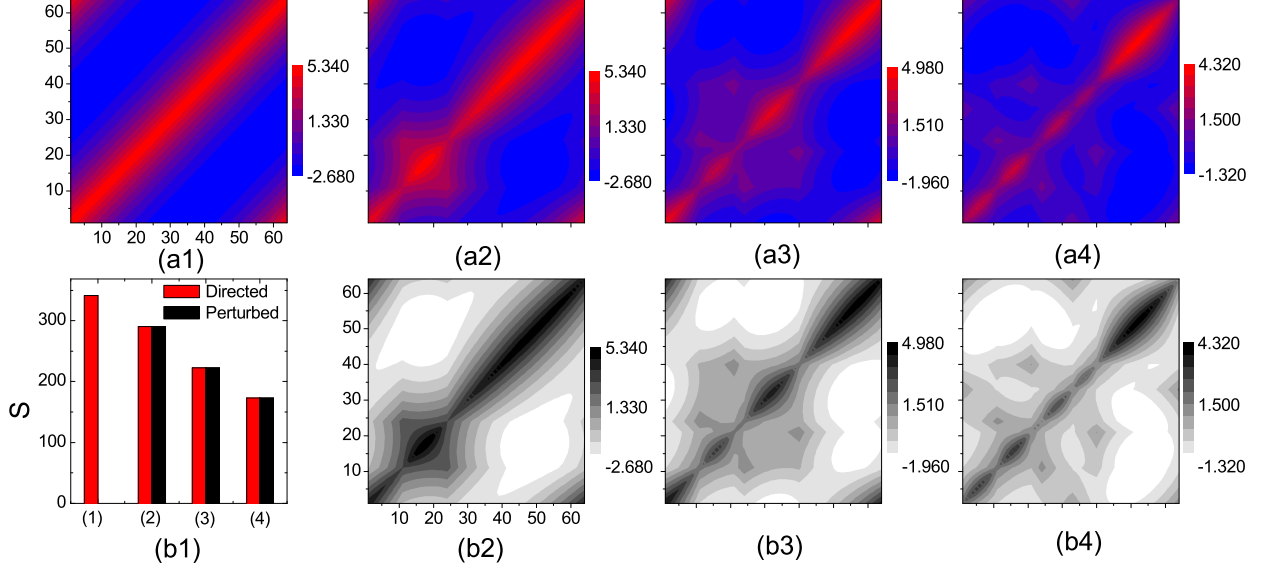


FIG. 1: (a1) The numerical result of the correlation of pairwise oscillator displacements on a ring chain $N = 64$. (a2) The numerical result of the correlation for adding link (11, 24) on (a1). (a3) is the numerical calculation of correlation for adding link (21, 40) on (a2). (a4) is the correlation for adding link (33, 64) on (a3). (b2), (b3), (b4) are the perturbed calculation results using Eq. (8), corresponding to their counterparts in the upper panel. (b1) shows the decreasing of S with adding cross-links. The red ones are calculated directly from numerical diagonalization and the black ones are the perturbed calculation using Eq. (8). All the results validate our analytic results.

This formula relates the dynamic vibration property S to the static structure property — the eigenvalue spectrum of Laplacian matrix L . When the average mean-square displacement S reaches the square of the typical spacing between oscillators, the structure encounters large vibrations and becomes unstable. Thus, small value of S means stable, while large value means unstable. It is clear that S has a trivial dependance on T and σ so that lower temperature or larger spring constant indicates more thermal stability. Therefore, to study the structure effect on S , we take $k_B T / \sigma = 1$ in the following, without loss of generality.

Based on Eq. (3) and (5), we can use exact numerical diagonalizations of the Laplacian matrix L to study the structure effect on thermodynamic stability.

In fact, the stability can be also studied by perturbation analysis, through which we find that the cross-links can suppress the thermodynamic instability, *i.e.*, decrease S effectively. After structure changes, the new Laplacian matrix is constructed as $L' = L - \Delta$, where Δ denotes the perturbation. The new correlation matrix C' can be written as

$$C' = (I - C\Delta)^{-1}C = C + C\Delta C + C\Delta C\Delta C + \dots \quad (6)$$

This is a standard algebraic algebra treatment of matrix perturbation, which can be simply regarded as Taylor series. In fact, it is similar to the Dyson equation in

Feynman-Dyson perturbation theory [9]. For the case of adding a link between nodes i and j , the perturbation matrix Δ can be expressed as

$$\Delta_{mn} = \delta_{mi}\delta_{nj} + \delta_{mj}\delta_{ni} - \delta_{mi}\delta_{ni} - \delta_{mj}\delta_{nj}. \quad (7)$$

Substituting the expression of Δ into C' , one obtains

$$C'_{mn} = C_{mn} - \frac{(C_{mi} - C_{mj})(C_{in} - C_{jn})}{1 + R_{ij}}, \quad (8)$$

where $R_{ij} = C_{ii} + C_{jj} - 2C_{ij} = \sum_{\alpha=1}^{N-1} (\psi_{\alpha i} - \psi_{\alpha j})^2 / \lambda_{\alpha}$. Therefore, the new average mean-square displacement is

$$\begin{aligned} S' &= \frac{1}{N} \text{tr} C' = S - \frac{\sum_{k=1}^N (C_{ik} - C_{jk})^2}{N(1 + R_{ij})} \\ &= S - \frac{1}{N(1 + R_{ij})} \sum_{k=1}^N \frac{(\psi_{\alpha i} - \psi_{\alpha j})^2}{\lambda_{\alpha}^2}. \end{aligned} \quad (9)$$

The second term in Eq. (9) is positive so that the value of new S' is always smaller than S . In other words, the cross-links always decrease S so as to increase the thermodynamic stability of the system. A specific case is studied and illustrated in Fig. 1.

In the following study, we choose a typical model to construct the small-world structure [10]. We first consider N oscillators (which might be an atom, a molecule,

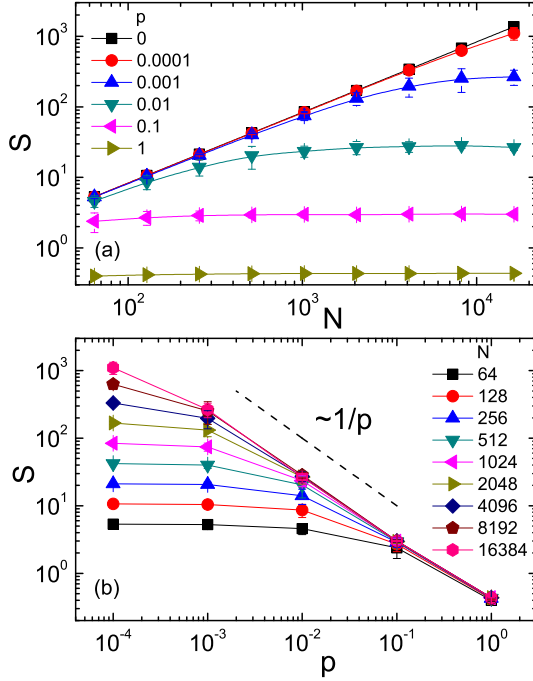


FIG. 2: (color online). (a) S versus network size N . The straight line for $p = 0$ indicates the diverging behavior, $S \sim N$, of the 1D ring chain. Even small nonzero value of p can suppress the diverging behavior of S and make it saturated to a finite value in the large size limit. (b) For each N , S decreases as p increases. A scaling behavior $S \sim 1/p$ emerges in the large size limit. All the results indicate that the cross-links boost the thermodynamic stability effectively.

or other module structure, depending on the system studied) on a one-dimensional(1D) ring chain, *i.e.*, with periodic boundary conditions. Each oscillator is connected to its nearest-neighbors. Then, we add a cross-link to each oscillator with probability p , which connects to another non-neighboring oscillator randomly. Thus, $E_{cr} = pN$ is the number of cross-links. When $p = 0$, the structure reduces to the 1D ring chain. In all cases studied below, each data point is obtained by averaging over 50 different network configurations for a given p and N .

Figure 2(a) illustrates S versus the system size N for different values of p in double logarithmic scale. The $p = 0$ case, corresponding to the 1D ring structure, shows the power-law divergence, $S \sim N$. It indicates that no thermodynamically stable solid exists at finite temperature in 1D. Indeed, when the average mean-square displacement S exceeds the square of the typical spacing between oscillators, the structure behaves like a liquid rather than a solid, and the crystalline order makes no sense anymore. This behavior is also reported in [11, 12]. For the case of $p \neq 0$, even of small value, as N increases,

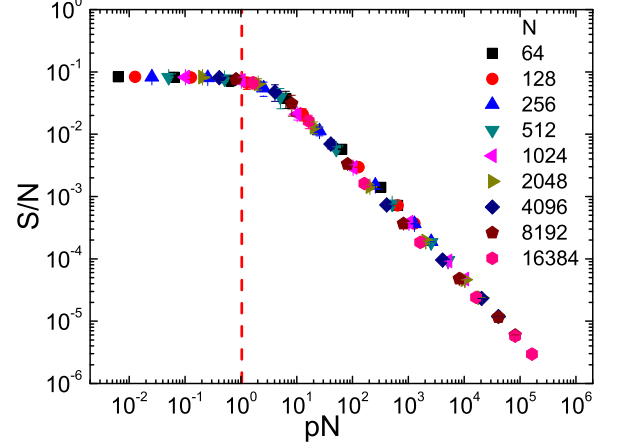


FIG. 3: (color online). Scaling plot of the average mean-square displacement S in small-world networks for various size N and probability p . All data are from Fig. 2 [13] and they collapse into one single line very well. It shows two phases clearly: one is the regime with slope -1 , where $p \gg 1/N$, indicating the non-divergent stable behavior $S/N \sim E_{cr}^{-1} = (pN)^{-1}$, *i.e.*, $S \sim 1/p$. Another one is the horizontal regime, indicating the diverging unstable behavior, $S \sim N$. The red vertical dashed line is used for eye-guiding to separate the two phases.

S is saturated to a finite value rapidly. Moreover, from Fig. 2(b), we can see that the larger p , the smaller S and in the large N limit, a scaling $S \sim p^{-1}$ emerges. All the above results indicate that the cross-links suppress the average mean-square displacement S effectively and make it convergent in the thermodynamic limit.

To eliminate the finite size effect, all the data from Fig. 2 [13] are re-scaled and the results are illustrated in Fig. 3. It is found that all data points collapse into one single line very well and two distinct phases emerge. For $p \ll 1/N$, there is a horizontal regime, $S/N \sim \text{const}$. It indicates an unstable phase: when the number of cross-links is smaller than one, S diverges with N . For $p \gg 1/N$, there is a regime with slope -1 , $S/N \sim E_{cr}^{-1} = (pN)^{-1}$, which indicates a convergent stable phase. In other words, when the number of cross-links is much larger than one, S approaches a finite value at large N and scales as p^{-1} .

Since the average mean-square displacement S is related to the spectral properties of the Laplacian matrix L , we can understand the scaling behavior of S in terms of its eigenvalue spectrum $\rho(\lambda)$. For large size N , Eq. (5) can be expressed as [12]:

$$S = \int \frac{\rho(\lambda)}{\lambda} d\lambda, \quad (10)$$

from which we can easily see that the density of small λ dominates the behavior of S . For the case without cross-links, the system reduces to a 1D ring chain,

where $\rho(\lambda) \sim \lambda^{-1/2}$ and $\lambda \sim N^{-2}$ for small λ . Thus, $S \sim \int \lambda^{-3/2} d\lambda \sim N$. For the case with cross-links, following the heuristic argument in [14], we can consider that the ring chain is divided into several quasi-linear segments of length l , and the probability of length l is exponentially small, e^{-pl} . Each segment l contributes to small eigenvalues of the order of l^{-2} . Summing over lengths with the exponential weight, we obtain $S = \int \frac{\rho(\lambda)}{\lambda} d\lambda \sim \int_0^N \frac{l^{-2} e^{-pl}}{1/l^2} dl = \frac{1}{p}(1 - e^{-pN})$. When $pN \ll 1$, $S \sim N$; while $pN \gg 1$, $S \sim 1/p$, which is exactly what our numerical results show in Fig. 2 and 3. Although the argument above is not rigorous and applies only when p is smaller than one, it gives us quite good understanding of the scaling behavior of S . When p is larger than one, the model we used is more like an Erdős-Rényi model, which is also to be demonstrated to follow the same scaling of the stable regime at the end of this paper.

The small-world structure we used above is well studied [10]. Using renormalization group method, the authors in Ref. [10] showed that this model undergoes a transition between regular lattice and random one at intermediate characteristic size $N_c \sim p^{-1}$. In other words, the phase transition has a critical point $p_c = 0$ in the thermodynamical limit when $N \rightarrow \infty$. For finite size N , the diameter l scales linearly with N for $N_c \gg N$ as it is in 1D ring chain, while $l \sim \ln N$ for $N \gg N_c$, where it exhibits “small-world” property. Our results about unstable and stable phases are consistent with their findings that the unstable regime corresponds to the 1D case and the stable phase corresponds to the “small-world” case.

As an illustrative example, the thermodynamic stability is further tested on real protein data. We revisit the proteins used in Ref. [2], which differ in functions and structures, with a wide size scale ranging from 100 to 3600 residues. All the structure data are downloaded from the Protein Data Bank (PDB) [15] and the number of all residue pairs is counted within a customary cut-off 7.0 Å. After eliminating the connectivity number of the primary structure of protein from the counted number, we obtain the number of cross-links, E_{cr} , for each protein. The mean square displacement of C^α atoms is characterized by B -factor [16], also called Debye-Waller or temperature factor: $B_i = 8\pi^2 \langle q_i^2 \rangle / 3$, where i is the index of amino acid residue. It is experimentally measured via x-ray crystallography, and also can be download from the PDB. The average B -factor is calculated over all C^α atoms for each protein, $B = \sum_{i=1}^N B_i / N$. Notice that at above theoretical analysis, $k_B T / \sigma$ is set to be 1 for convenience, which is not always true. The value of $k_B T / \sigma$ varies among different proteins. Thus, we use the estimated data of $k_B T / \sigma$ [2] to obtain the normalized average B -factor, $B' = B / (k_B T / \sigma)$. Note that B' is analogous to S , defined in Eq. (10). All the details of these proteins are listed in Table I in Appendix B.

The thermodynamic stability is crucial to keep the native structure of protein for right function. Moreover the structure of protein is also found to have “small-world”

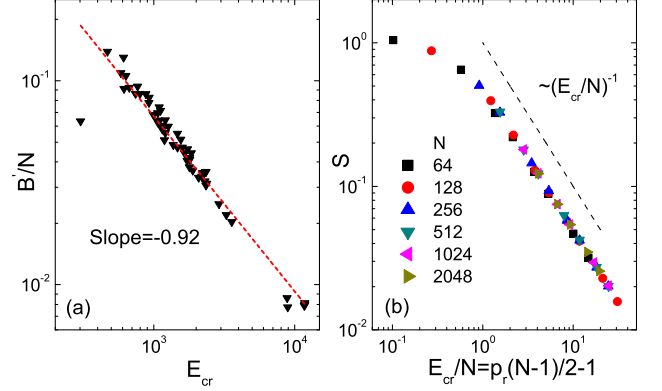


FIG. 4: (color online). (a) Log-log plot of normalized average B -factor with various number of cross-links for real protein data. It exhibits clearly a power-law behavior, $B'/N \sim E_{cr}^{-a}$. The dashed line indicates the best-fit of the power-law, with exponent $a = -0.92 \pm 0.01$. (b) The average mean-square displacement S versus the parameter $E_{cr}/N = p_r(N-1)/2-1$ in Erdős-Rényi model. The dashed line indicates the scaling.

property [17], *i.e.*, $l \sim \ln N$. It is intuitive for us to expect that nature selection forces proteins evolving into the stable phase in Fig. 3, which implies $B'/N \sim E_{cr}^{-1}$. Figure 4(a) verifies our expectation drawn from the argument of stability analysis. In fact, we obtain a clear power-law scaling:

$$B'/N \sim E_{cr}^{-a}, \quad a = 0.92 \pm 0.01, \quad (11)$$

which is quite close to 1. This scaling reveals the universal behavior shared by various different proteins, regardless of their sources or functions. It implies an underlying general mechanism that nature selects proteins with thermodynamic stability constraints.

Although protein has more complex structures with high modularity(domains), “small-world” property captures its main feature. Thus, “small-world” might play a key role in the thermodynamic stability of structures and be responsible for the scaling in the stable regime. To validate our conjecture, we further study the thermodynamic stability in Erdős-Rényi(ER) random network model in the following.

ER model [18] has N nodes and every pair of nodes is connected with probability p_r . The average degree $\langle k \rangle = p_r(N-1)$. There are several phases in this model depending on different threshold p_r : when $\langle k \rangle = p_r(N-1) > 3.5$ [18], the diameter of the graph equals the diameter of the giant cluster, and is proportional to $\ln N$, *i.e.*, “small-world” property. Thus, it is straightforward to expect that ER model might share the same behavior $S/N \sim E_{cr}^{-1}$. The numerical result is illustrated in Fig. 4(b). As we point out above, ER model has “small-world” property [19] when $p_r(N-1) > 3.5$. Correspondingly, when $p_r(N-1)/2-1 > 0.75$, $S \sim N/E_{cr} =$

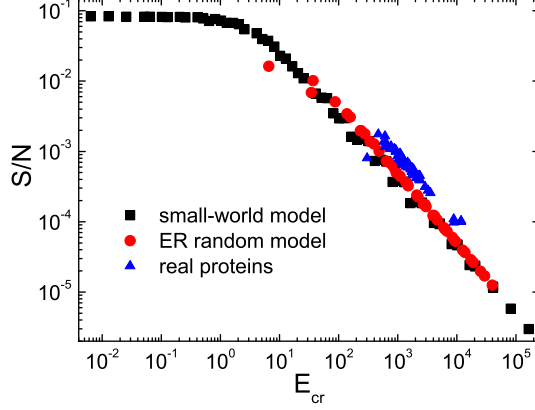


FIG. 5: (color online). S/N versus E_{cr} for three different networks. It shows that the “small-world” property is responsible for the universal scaling $S/N \sim E_{cr}^{-1}$ in the stable regime, regardless of the model details. Note that for proteins, $S = B'/(8\pi^2)$, where the factor 3 is removed since B -factor is measured in 3-dimension.

$N/(p_r N(N-1)/2 - N) = [p_r(N-1)/2 - 1]^{-1}$ as shown in Fig. 4(b).

For convenience of comparison, we plot the data of three cases together in Fig. 5. It clearly shows the universal scaling $S/N \sim E_{cr}^{-1}$ in the regime where the three structures all have “small-world” property, $l \sim \ln N$. Moreover, we have tested other network models [20] sharing the property $l \sim \ln N$. The results indicate that the “small-world” property plays the key role in the stable regime and is responsible for the universal scaling, regardless of the model details, which can be explained in the framework of a mean-field approach [20].

In summary, we have studied the vibrational thermodynamic stability of small-world structures. The average mean-square displacement S of the structure has been expressed as the mean of inverse eigenvalues of its Laplacian matrix L . Therefore, the dynamic vibration property is closely related to the static structure information. It is found that the cross-links suppress S effectively and on the small-world network model, there exist two phases: an unstable phase where $p \ll 1/N$, $S \sim N$ and a stable phase where $p \gg 1/N$, $S \sim p^{-1}$, *i.e.*, $S/N \sim E_{cr}^{-1}$. Further, we have tested various data from the PDB and find that native proteins belong to the stable phase and share the same scaling behavior $S/N \sim E_{cr}^{-1}$. It is believed that nature selects proteins under the constraint of thermodynamic stability so that proteins can keep their specific native fold structure stable for proper function. Finally, we have studied S in ER random network model and have validated our conjecture that it is the “small-world” property that plays a key role in the thermodynamic stability of structures and is responsible for the universal scaling, $S/N \sim E_{cr}^{-1}$, in the stable regime. It is also interesting to examine more complex structure

effects on the thermodynamic stability problem, such as scale-free networks [20], hierarchical structures, networks with community structure *etc.* More realistic considerations such as the effect of random coupling constants, anharmonic potentials, or even quantum version of vibration dynamics are worth further studying.

The work is supported by the NUS Faculty Research Grant No. R-144-000-165-112/101.

APPENDIX A: DERIVATION OF THE CORRELATION MATRIX

To make this paper self-contained and readable, we complement the detailed derivation of Eq. (2) which is expressed in terms of G in Fourier transform space. We follow Ref. [21] by defining the Fourier transform as

$$Q(\omega) = \frac{1}{2\pi} \int_{-\infty}^{+\infty} q(t) e^{-i\omega t} dt; \quad (\text{A1})$$

$$\eta(\omega) = \frac{1}{2\pi} \int_{-\infty}^{+\infty} \xi(t) e^{-i\omega t} dt. \quad (\text{A2})$$

Applying Fourier transform to both sides of Eq. (1), one obtains

$$-\omega^2 M Q = -\sigma L Q - i\omega \Gamma Q + \eta. \quad (\text{A3})$$

Simple algebraic operation yields,

$$Q = G^{-1}(i\omega) \eta, \quad (\text{A4})$$

where matrix $G(i\omega) = -\omega^2 M + i\omega \Gamma + \sigma L$ as defined in text. The two point correlation function is

$$\begin{aligned} & \langle q_l(t+\tau) q_k(t) \rangle \\ &= \int_{-\infty}^{+\infty} d\omega e^{i\omega(t+\tau)} \int_{-\infty}^{+\infty} d\omega' e^{-i\omega' t} \langle Q_l(\omega) Q_k^*(\omega') \rangle \\ &= \int_{-\infty}^{+\infty} d\omega e^{i\omega(t+\tau)} \int_{-\infty}^{+\infty} d\omega' e^{-i\omega' t} \\ & \quad \times \langle \eta(\omega) \eta^*(\omega') \rangle [G^{-1}(i\omega) G^{-1}(-i\omega')]_{lk}. \end{aligned} \quad (\text{A5})$$

where $*$ denotes the conjugate transpose and $Q^*(\omega') = \eta^*(\omega') G^{-1}(-i\omega')$. Moreover, since

$$\begin{aligned} \langle \eta(\omega) \eta^*(\omega') \rangle &= \frac{1}{2\pi} \int_{-\infty}^{+\infty} dt e^{-i\omega t} \\ & \quad \times \frac{1}{2\pi} \int_{-\infty}^{+\infty} dt' e^{i\omega' t'} \langle \xi(t) \xi^*(t') \rangle \\ &= \frac{k_B T \Gamma}{\pi} \frac{1}{2\pi} \int_{-\infty}^{+\infty} e^{i(\omega' - \omega)t} dt \\ &= \frac{k_B T \Gamma}{\pi} \delta(\omega' - \omega), \end{aligned} \quad (\text{A6})$$

substitute Eq. (A6) into Eq. (A5) and we have:

$$\begin{aligned} & \langle q_l(t+\tau) q_k(t) \rangle \\ &= \frac{k_B T}{\pi} \int_{-\infty}^{+\infty} d\omega e^{i\omega \tau} [G^{-1}(i\omega) \Gamma G^{-1}(-i\omega)]_{lk}. \end{aligned} \quad (\text{A7})$$

The expression of correlation matrix Eq. (2) corresponds to the special case $\tau = 0$.

APPENDIX B: INFORMATION OF PROTEINS

PDB code	N	E_{cr}	B	$k_B T/\sigma$	B'/N	PDB code	N	E_{cr}	B	$k_B T/\sigma$	B'/N
9RNT	104	303	10.9147	1.657	0.06334	16PK	415	1472	14.3769	0.63	0.05499
1BVC	153	469	8.33124	0.392	0.13891	1BU8	446	1559	19.7459	0.859	0.05154
1G12	167	584	14.4393	0.793	0.10903	1AC5	483	1598	24.8104	1.091	0.04708
1AMM	174	612	0.06793	0.003	0.13013	1LAM	484	1737	10.9112	0.488	0.0462
1KNB	186	616	18.7711	1.104	0.09141	1CPU	495	1659	13.5504	0.62	0.04415
1CUS	197	671	16.6598	0.914	0.09252	3COX	500	1792	9.2601	0.491	0.03772
1IQQ	200	634	10.164	0.48	0.10588	1A65	504	1724	21.3040	1.042	0.04057
2AYH	214	744	9.9678	0.539	0.08642	1SOM	528	1805	34.3889	1.585	0.04109
1AE5	223	768	19.9342	0.952	0.09390	1E3Q	534	1799	35.0785	1.577	0.04181
1LST	239	799	20.2462	0.982	0.08627	1CRL	534	1893	18.7736	0.969	0.03628
1A06	279	880	52.5323	2.184	0.08621	1AKN	547	1851	41.9999	1.737	0.0442
1NAR	289	925	13.5809	0.602	0.07806	1CF3	581	2082	22.4561	1.154	0.03349
1A48	298	928	16.3599	0.664	0.08268	1EX1	602	2199	24.2479	1.193	0.03376
1A3H	300	1076	13.4101	0.719	0.06217	1A14	612	2198	17.9869	0.865	0.03398
1SBP	309	1061	12.5878	0.641	0.06355	1MZ5	622	2234	16.4778	0.75	0.03532
1A5Z	312	1070	45.6872	2.111	0.06937	1CB8	674	2348	28.0511	1.164	0.03575
1A1S	313	1088	21.3477	1.068	0.06386	1HMU	674	2341	21.8915	0.907	0.03581
1ADS	315	993	10.7205	0.5	0.06807	1A47	683	2350	13.5361	0.646	0.03068
1A40	321	1153	9.72025	0.524	0.05779	1CDG	686	2375	23.1041	1.074	0.03136
1A54	321	1144	11.6098	0.601	0.06018	1DMT	696	2313	26.9702	1.204	0.03218
1A0I	332	1094	27.2887	1.109	0.07412	1A4G	780	2904	11.4584	0.591	0.02486
3PTE	347	1210	8.13032	0.366	0.06402	1HTY	988	3276	14.0281	0.646	0.02198
1A26	351	1117	34.2736	1.369	0.07133	1KCW	1017	3579	44.0269	2.13	0.02032
1BVW	360	1209	13.0188	0.652	0.05547	1KEK	2462	8860	26.7142	1.263	0.00859
8JDW	360	1191	23.8334	1.293	0.05120	1B0P	2462	8936	6.08348	0.319	0.00775
7ODC	387	1266	19.8278	0.859	0.05964	1K83	3490	11725	55.9118	2.03	0.00788
1OYC	399	1378	20.4127	1.056	0.04845	1I3Q	3542	11813	70.0899	2.435	0.00813
1A39	410	1474	21.4742	1.113	0.04706	1I50	3558	11799	63.2545	2.236	0.00795

TABLE I: Information of Proteins used in the present study. Size N is the number of residues. E_{cr} is the number of cross-links, counted within cutoff 7 Å. B is the average B -factor over all C^α atoms for each protein. The estimated $k_B T/\sigma$ are collected in Ref. [2]. B'/N is the normalized B -factor over the size of protein.

-
- [1] C. Kittel, *Introduction to Solid State Physics*, (John Wiley, Singapore, 1996).
- [2] R. Burioni, D. Cassi, F. Cecconi, and A. Vulpiani, *Proteins: Struct. Funct. Bioinf.* **55**, 529 (2004).
- [3] S. Reuveni, R. Granek, and J. Klafter, *Phys. Rev. Lett.* **100**, 208101 (2008).
- [4] D.J. Watts and S.H. Strogatz, *Nature* **393**, 440 (1998).
- [5] M.M. Tirion, *Phys. Rev. Lett.* **77**, 1905 (1996).
- [6] T. Haliloglu, I. Bahar, and B. Erman, *Phys. Rev. Lett.* **79**, 3090 (1997); I. Bahar, A.R. Atilgan, and B. Erman, *Folding Des.* **2**, 173 (1997); Q. Cui and I. Bahar, *Normal Mode Analysis*, (Chapman&Hall/CRC, London, 2006).
- [7] P.J. Flory, *Proc. R. Soc. London A* **351**, 351 (1976).
- [8] D.S. Pearson, *Macromolecules* **10**, 696 (1977).
- [9] G.D. Mahan, *Many-Particle Physics*, (Plenum Press, New York, 2000).
- [10] M.E.J. Newman and D.J. Watts, *Phys. Lett. A* **263**, 341 (1999).
- [11] R. Peierls, *Helv. Phys. Acta* **7**, Suppl. 2, 81 (1934).
- [12] R. Burioni, D. Cassi, M.P. Fontana, and A. Vulpiani, *Europhys. Lett.* **58**, 806 (2002).
- [13] We add two more cases ($p = 5$ and $p = 10$) for all sizes. Here, p is larger than one, which means adding to each oscillator p cross-links on average.
- [14] A.J. Bray and G.J. Rodgers, *Phys. Rev. B* **38**, 11461 (1988); R. Monasson, *Eur. Phys. J. B* **12**, 555 (1999).
- [15] F.C. Bernstein *et al.*, *J. Mol. Biol.* **112**, 535 (1977).
- [16] U.G. Wagner *et al.*, *J. Mol. Biol.* **247**, 326 (1995).

- [17] M. Vendruscolo, N.V. Dokholyan, E. Paci, and M. Karplus, Phys. Rev. E **65**, 061910 (2002); A.R. Atilgan, P. Akan, and C. Baysal, Biophys J. **86**, 85, (2004).
- [18] B. Bollobás, Random Graphs (Academic Press, New York, 1985).
- [19] Note that in this paper, we only refer to the “small-world” property to short average path length, *i.e.*, $l \sim \ln N$, although the “small-world” properties used nowadays include the additional property of high clustering, after Ref. [4].
- [20] J. Ren and B. Li (in preparation).
- [21] R. Kubo, M. Toda, and N. Hashitsume, *Statistical Physics II*, (Springer, New York, 1991).